Journal of Electroanalytical Chemistry, 369 (1994) 131–144

A quantum chemistry description of carbon monoxide and water absorbates on single-crystal rhodium and platinum clusters

P. Paredes Olivera, G. Estiu, E.A. Castro and A.J. Arvia *

Instituto de Investigaciones Fisicoquímicas Teóricas y Aplicadas (INIFTA), Facultad de Ciencias Exactas, Universidad Nacional de La Plata, Sucursal 4, Casilla de Correo 16, (1900) La Plata (Argentina)

(Received 13 January 1992, in revised form 31 August 1993)

Abstract

Extended Huckel molecular-orbital calculations of CO and HO adsorbed ensembles on single-crystal Pt and Rh clusters are presented The energy ranges related to the stability of adsorbed ensembles of the type $(Me)_N(CO)_n(OH)_m$, where Me stands for Rh(100), Rh(111), Pt(100) and Pt(111), were calculated for various coordination geometries and applied potential conditions A stability inversion potential was found for each ensemble A correlation was obtained between the stability inversion potentials resulting from the different adsorbed ensembles and the potentials of the current peaks related to the voltammetric oxidation of CO adsorbates on Pt and Rh resulting from comparable potential perturbation conditions

1. Introduction

The chemisorption of CO on noble metals such as Rh and Pt in acid solutions is of particular interest with respect to C1 chemistry [1–5] because CO acts as a poison in the catalytic oxidation of organic compounds such as methanol, formic acid and hydrocarbons by occupying active surface sites [6]

The electrocatalytic properties of Rh and Pt, which are known from the study of several electrochemical reactions, appear to be rather similar [7,8] In the absence of specific metal complexing species, Rh and Pt behave as stable materials at all pH values in aqueous solutions, although the electrochemical oxidation of Rh takes place at a potential lower than that of Pt [9,10] Data derived from ultrahigh vacuum (UHV) measurements [11,12] for these two metals have shown that different metal–adsorbate and lateral adsorbate–adsorbate interactions occur for those adsorbed intermediates which are involved in a number of catalytic oxidation reactions on Rh and Pt surfaces [13] A comprehensive understanding of the structure of CO adsorbates on Pt and Rh is required to improve the electrocatalytic performance of these metals [14–17]

Electrochemical [18–21] and UHV gas phase data [22–27] demonstrate that CO adsorbs on both Rh and Pt surfaces in linear and bridge forms, and the surface concentration ratio of these forms depends on θ_{CO}, the degree of metal surface covered by CO, and the electronic characteristics of the metal surface, which are determined by the nature and the topography of the metal as well as the applied potential for electrochemical systems In these cases, for potentials lying in the range where CO electro-oxidation on Pt takes place, the CO bridge adsorbate configuration is almost absent [28]

Since the anodic stripping voltammograms for CO adsorbates on Rh and Pt in aqueous electrolyte solutions are very different (Figs 1 and 2) [18–20], it has been concluded that the adsorption energy difference between the bridge and linear forms of CO adsorbates on Pt is larger than that on Rh Accordingly, the interconversion between the two forms of CO on Rh will be easier than on Pt, giving rise to a single CO anodic stripping current peak for Rh (Fig 2) instead of the current peak multiplicity found for Pt (Fig 1) [20]

Generally, CO adsorbate structures on noble metals in electrochemical systems have been described as coadsorbed complex ensembles [19,20], consisting of CO and OH species on well-defined Pt sites The presence of OH species results from the fast electro-

* To whom correspondence should be addressed

0022-0728/94/$7 00
SSDI 0022-0728(93)03133-A

© 1994 – Elsevier Sequoia All rights reserved

oxidation of H_2O which takes place at potentials slightly less positive than the CO adsorbate electro-oxidation threshold potential Based upon of the existence of these adsorbed structures, a first molecular orbital explanation of the origin of the adsorbed CO electro-oxidation voltammetric current peaks in acid solution in the absence of anion specific adsorption on Pt(100) and Pt(111) [29], and on Rh(111) [30] has been advanced

Recent experimental [31–38] and theoretical [39–44] investigations of the mechanism of the CO electro-oxidation reaction have confirmed that two main CO adsorbate coordination geometries are present on Pt and Rh surfaces However, recent experimental research has suggested different interpretations of the interaction of CO on noble metal surfaces, and a nucleation and growth mechanism, which implies the formation of CO islands on the metal substrate, has been proposed [45–50] Regardless of the model, it is generally accepted that the CO adsorbate oxidizing agent is either OH or water molecules adjacent to the CO adsorption sites [45,51]

The first molecular orbital interpretation of adsorbed CO electro-oxidation on Pt surfaces was based on the existence of lateral interactions between CO and OH adsorbates at adjacent sites, disregarding the possibility of a nucleation and growth mechanism

This paper is the last in a series [31,32] devoted to a possible interpretation of the electro-oxidation of CO adsorbates formed on noble metals (Me) on the basis of the stability of the $[Me]_N(OH)_n(CO)_m$ ensembles formed on Pt(111), Pt(100), Rh(111) and Rh(100) as a function of the applied potential The calculation procedure describes the influence of the electronic characteristics of the metal surfaces on the stability of CO adsorbates on these noble metals Results indicate that the difference in the electrochemical electro-oxidation of adsorbed CO on Pt and Rh single crystals is due partly to the different adsorptive properties of the two metals with respect to CO, and partly to the potential ranges of stability of H and OH adsorbed species, resulting from the electrochemical decomposition of water, on the metals It should be noted that the potential range where CO and H coadsorption takes

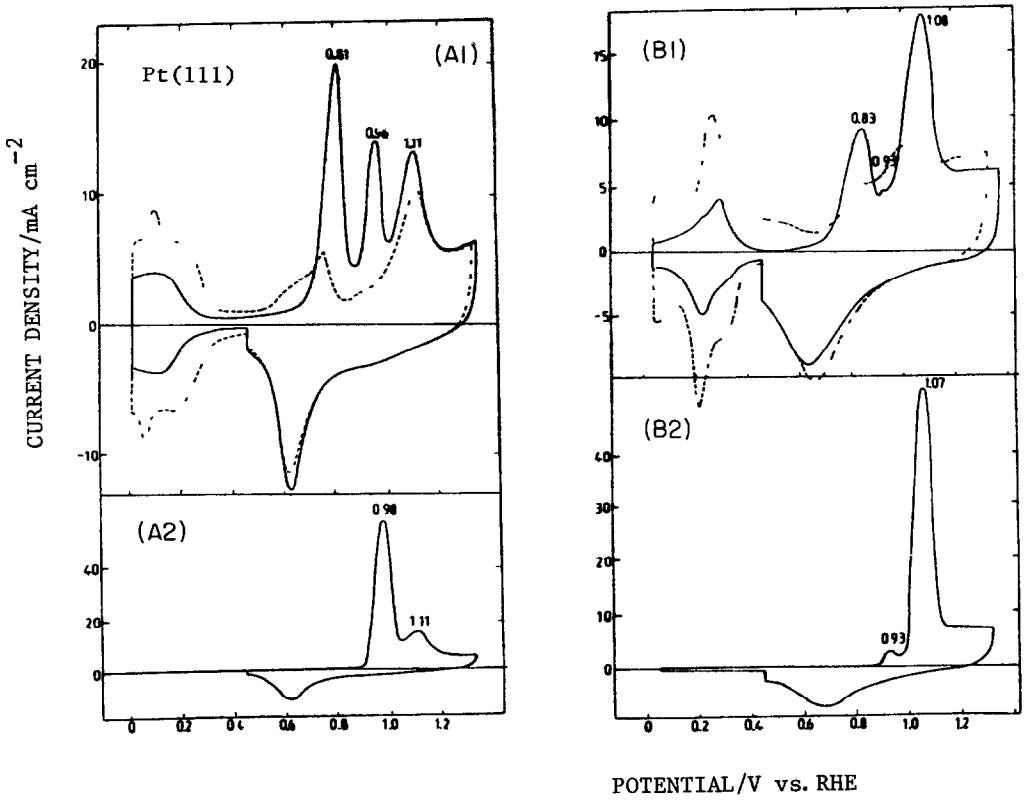

Fig 1 Voltammograms related to the electro-oxidation of CO adsorbates on (A) Pt(111) and (B) Pt(100) single-crystal electrodes at 10 V s^{-1} in CO-saturated 0 5 M $HClO_4$ at a CO adsorption potential E_{ads} of 0 45 V/(RHE) and different adsorption times τ_{ads} at 25°C (A1) $\tau_{ads} = 2\,6$ s (full curve), and blank (broken curve), (A2) $\tau_{ads} = 25$ s, (B1) $\tau_{ads} = 2\,8$ s (full curve) and blank (broken curve), (B2) $\tau_{ads} = 20$ s Data taken from ref 2 with permission of Elsevier Science Publishers

place on Rh is larger than that on Pt [20] We understand that the conclusions derived from molecular orbital calculations are compatible with the nucleation and growth model, as the proposed CO adsorption geometries are valid for the first layer of the adsorbed nucleus

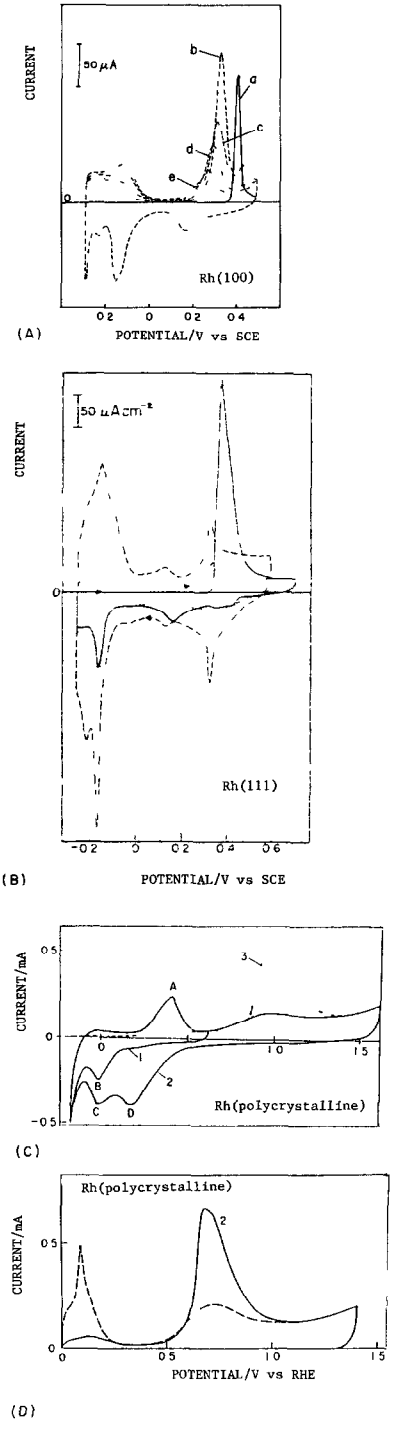

This work covers the following topics The calculation procedure and experimental literature data are reviewed in Sections 2 and 3 The dependence of the possible CO adsorbate configurations on the electronic characteristics of the metal surface is discussed in Section 4 Finally, in Sections 5 and 6 a correlation is attempted between the stability inversion potentials resulting from the different adsorbed ensembles, and the anodic stripping potentials of CO adsorbates on Pt and Rh

2. Outline of the calculation procedure

The value of the energy E related to chemical bond formation is given by the sum of two energy components E_R and E_{MO} E_R is a pairwise atom–atom repulsive energy term and E_{MO} is an attractive energy term due to electron delocalization and bond formation Following the procedure of Anderson and coworkers [52,53], this energy has been approximated as a sum of one-electron molecular orbital energies obtained by diagonalizing a Hamiltonian similar in form to the extended Huckel Hamiltonian

The method can be described briefly as follows The energy matrix elements of the attractive energy component were calculated from the equations [52]

$$H_{ii}^{aa} = -(\mathrm{VSIP})_i^a \tag{1}$$

$$H_{ij}^{aa} = 0 \tag{2}$$

$$H_{ij}^{ab} = 1\,125\left(H_{ii}^{aa} + H_{jj}^{bb}\right)S_{ij}^{ab}\exp(-0\,13R) \tag{3}$$

where the i run over all orbitals and the a run over all atoms, VSIP denotes the valence state ionization potential, S_{ij}^{ab} is the overlap integral between orbital i on centre a and orbital j on centre b, and R is the internuclear distance between centres a and b The values of S_{ij}^{ab} were calculated using Slater-type valence orbitals The exponents of the Slater orbitals were taken from the literature [54]

Core–core repulsive energy values E_R were calculated as pairwise additive in the way proposed by Anders et al [55]

Fig 2 Voltammograms related to the electro-oxidation of CO adsorbates at 0 05 V s^{-1} on different Rh electrodes (A) Rh(100) in 0 1 M $HClO_4$ (a) $\theta_{CO} = 0\,77$, (b) $\theta_{CO} = 0\,45$, (c) $\theta_{CO} = 0\,3$, (d) $\theta_{CO} = 0\,2$, (e) $\theta_{CO} = 0\,1$ The current scale voltammogram (a) is fourfold compressed (B) Rh(111) in 0 1 M $HClO_4$ $E_{ads} = -0\,25$ V (full curve), blank (dotted curve) The broken curve corresponds to the blank with a current scale magnified 2 5 times (C) Polycrystalline Rh in 0 2 M K_2SO_4 The broken curve corresponds to the blank (D) Polycrystalline Rh in 0 5 M H_2SO_4 in the absence (dashed line) and presence (solid line) of an adsorbed CO monolayer Data from refs 21, 29 and 30 by permission of Elsevier Science Publishers and The American Chemical Society

The binding energy (BE) between a complex adsorbate such as $(CO)_n(OH)_m$ consisting of an ensemble of n CO and m OH species on a substrate metal site $[Me]_N$ formed by N metal atoms, is defined as follows

$$BE = E_{[Me]_N(CO)_n(OH)_m} - nE_{(CO)} - mE_{(OH)} - E_{[Me]_N} \quad (4)$$

where the E denote the energies of the different ensembles

To reproduce the work function modification due to adsorption, the initial values of VSIPs given in refs 56 and 57 were adjusted until the charge transfer at the equilibrium distance in the heteronuclear diatomic bond was close to that predicted by the electronegativity difference in Pauling's ionicity relationship [58]

The charge transfer reaction

$$[Me] + H_2O = [Me](OH) + H^+ + e^- \quad (5)$$

involving the reversible electroadsorption of the water molecule on the metal defines the equilibrium electrode potential The charge transfer induced by the O atom is larger than that induced by the C atom bonded to the metal Consequently, the VSIPs of this system were taken as a reference for simulating the electric potential applied to the electrochemical interface A positive applied electric potential shifts the Fermi level of the metal downwards in the energy scale and vice versa Thus these changes were simulated by either decreasing or increasing the VSIPs of the metal from the reference values associated with the equilibrium electrode potential defined by eqn (5) The values of VSIPs and Slater orbital exponents employed in the calculations are given in Table 1

It should be noted that a 1 V shift in the applied electric potential does not necessarily correspond to a 1 eV shift in VSIP In earlier work it was found that a correlation $g \approx 0\,3$ eV V^{-1} allowed a reasonable description of the energy range of stable CO adsorbate structures on Pt(111) ($g = 0\,32$) [31] and Rh(111) ($g = 0\,30$) [32] This value of g could be justified from ESCA measurements at the Au(100) + 0 5 M NaF system [59,60] For this system a 1 0 V shift in the energy of bulk states was related to a 0 3 eV shift in surface state energy [59,60] The shift in Fermi energy level with the applied electric potential differs appreciably for various metal|electrolyte solution interfaces, as is expected since the characteristics of the correlation are determined by both surface and bulk state energies, which in turn exhibit specific responses to the applied electric potential For example, in contrast with $g = 0\,3$ eV V^{-1} for Au(100) + 0 5 M NaF, the value of g for the Ag(110) + 0 5 M NaF system ranges from 3 to 4 eV V^{-1} [61] In the case we are studying, the electronic structure of the surface, defined by the nature and topology of the metal, has an influence on the g value, as shown in Table 2

Clusters $[Me(111)]_{22}$ and $[Me(100)]_{25}$ with d bands filled with at least one electron per orbital were used to model the single-crystal metal surfaces (Fig 3) The clusters were constructed geometrically from the Rh–Rh and Pt–Pt closest approach distances (0 2687 nm and 0 2770 nm respectively) The smallest cluster dimension compatible with the minimum influence of border effects was used to model the adsorption systems Accordingly, cooperative interactions between adsorbates on the central four-atom region of the cluster were considered (Figs 4 and 5)

The Me–CO and Me–OH adsorption bond lengths were calculated from the minimum of binding energy versus Me–adsorbate distance curves A linear configuration perpendicular to the metal surface was considered for both CO and OH in the coadsorbed systems on the basis of the adsorption geometries of the species separately [19,31] The C–O and O–H interatomic distances were fixed at 0 116 nm and 0 100 nm respectively The OH species adsorbed at 0 195 nm from the Rh(111) surface and 0 20 nm from the Pt(111) surface,

TABLE 1 Parameters used in the calculations principal quantum number n for s, p and d orbitals, orbital exponent ξ, ionization potential VSIP and coefficients C_1 and C_2 for d orbitals

Atom		s orbital			p orbital			d orbital					
		n	ξ	VSIP	n	ξ	VSIP	n	ξ_1	VSIP	C_1	C_2	ξ_2
O	(A)	2	1 946	−26 98	2	1 927	−12 12						
	(B)	2	2 146	−26 98	2	2 127	−12 12						
H	(A)	1	1 000	−12 10									
C	(B)	2	1 658	−18 50	2	1 618	−9 760						
Rh	(C)	5	2 135	−9 670	5	2 100	−6 314	4	4 290	−11 77	0 5807	5 686	1 970
Pt	(C)	6	2 850	−10 99	6	2 550	−6 955	5	6 310	−11 59	0 6640	0 5779	2 410

(A) Atom in H_2O molecule
(B) Atom in CO molecule
(C) Me in either $[Me(100)]_{25}(H_2O)(CO)$ or $[Me(111)]_{22}(H_2O)(CO)$ ensembles

TABLE 2 Correlation between SIP values of different CO adsorbates on Me(111) or Me(100) (Me = Pt (A) or Rh (B)) and the potentials of the CO electro-oxidation voltammetric peaks recorded at constant potential sweep v

	SIP (calc) /eV	g [a] /eV V^{-1}	EOP (calc) /V	EOP (exp) /V
Me = Pt				
Pt(111)CO^T Figs 4 1(a), 4 1(d)	0 25	0 32	0 78	0 81
Pt(111)CO^T Figs 4 1(b), 4 1(e)	0 30	0 32	0 94	0 96
Pt(111)CO^T Figs 4 1(c), 4 1(f)	0 35	0 32	1 09	1 11
Pt(111)CO^B Fig 4 2(a), 4 2(b)	0 39	0 32	1 21	–
Pt(100)CO^T Fig 5 1(b), 5 1(f)	0 23	0 27	0 85	0 83
Pt(100)CO^T Fig 5 1(c), 5 1(f)	0 25	0 27	0 93	0 93
Pt(100)CO^T Fig 5 1(d), 5 1(g)	0 31	0 27	1 14	1 08
Me = Rh				
Rh(111)CO^T Fig 4 1(a), 4 1(d)	0 14	0 29	0 48	0 47
Rh(111)CO^T Fig 4 1(b), 4 1(e)	0 22	0 29	0 76	0 75
Rh(111)CO^H Fig 4 3(a), 4 3(b)	0 48	0 29	1 65	1 62
Rh(100)CO^T Fig 5 1(a), 5 1(e)	0 24	0 31	0 77	0 75
Rh(100)CO^T Fig 5 1(b), 5 1(f)	0 30	0 31	0 97	0 95
Rh(100)CO^T Fig 5 1(c), 5 1(f)	0 43	0 31	1 38	–
Rh(100)CO^T Fig 5 1(d), 5 1(g)	0 44	0 31	1 41	–
Rh(100)CO^B Fig 5 2(a), 5 2(b)	0 29	0 31	0 94	0 95

The values indicate the probable adsorbate involved at different electro-oxidation potentials Calculated (calc) and experimental (exp) EOP values are given The relation between EOP (calc), SIP (calc) and g, as well as the definition of g, are given in the text

[a] $v = 10$ V s^{-1} for Pt and $v = 0\,05$ V s^{-1} for Rh

whereas in the presence of adsorbed OH the CO molecule is stabilized at 0 224 nm from the Rh(111) surface and 0 213 nm from the Pt(111) surface

3. Adsorbed CO voltammetric electro-oxidation on Rh and Pt: summary of the experimental data

The electrochemical oxidation of CO adsorbates in acid electrolytes has been investigated on Rh [21] and more extensively on Pt single crystals and Pt polycrystalline electrodes [1,2,18,19] for different values of θ_{CO} Recently, absolute surface IR spectra for CO on Rh(100) and Rh(111) [29,30] and on Pt(111) and Pt(100) [37] in acid solution have also been reported as a function of θ_{CO} and the electrode potential V

The electro-oxidation of adsorbed CO on Pt and Rh (Figs 1 and 2) in aqueous solution behaves as a typical irreversible electrochemical process The reaction taking place on these metals exhibits some common features, namely the multiplicity and position of the corresponding voltammetric peaks depend strongly on θ_{CO}, the crystal face of the metal and the electrolyte composition including pH Thus, for $\theta_{CO} \approx 0\,5$, two CO electro-oxidation peaks were found for Pt(100) and Pt(111) in acid media In contrast, for $\theta_{CO} \approx 1$, a single sharp anodic voltammetric peak located at a high positive potential was observed

However, on polycrystalline Rh with $\theta_{CO} \approx 1$, the electro-oxidation of adsorbed CO in acid exhibits a single, although somewhat distorted, anodic peak (Fig 2A) probably involving a complex structure The characteristics of this peak agree with the pseudo-derivative shape of the corresponding electromodulated IR spectral (EMIRS) band [30] Furthermore, the features of the anodic peak depend on whether the reaction takes place on Rh(100) or Rh(111) (Fig 2B) In the former case, the shift of the peak potential to lower values as θ_{CO} is decreased from 0 77 to 0 1 suggested the existence of two distinguishable types of CO adsorbates on Rh in acids

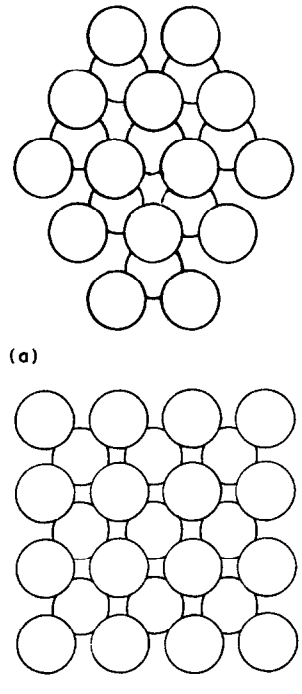

Fig 3 Cluster models for the different Me surface sites (a) Me(111), (b) Me(100) Me = Rh, Pt

The existence of different CO adsorption bonds has been concluded from UHV data for Rh/CO(gas) and Pt/CO(gas) systems [22–27] The latter were also used to describe the electrochemical behaviour of CO Thus the anodic peak for Pt at low potentials was associated with bridge-bonded (bicoordinated) CO, whereas the peak at high potentials was attributed to linearly bonded CO [2,3] The origin of the single desorption voltammetric peak obtained on polycrystalline Rh [21] was assigned exclusively to the presence of linearly bonded CO produced by the interconversion from facile bridge to linear adsorbate at the Rh surface However, this explanation disagrees with gas phase spectroscopic data which suggest that only linearly bonded CO is present on Rh for $\theta_{CO} \Rightarrow 1$ The oxidative desorption of CO adsorbates from both Rh and Pt has been explained in terms of a mechanism of lateral interactions between CO and oxygenated intermediates adsorbed on the metal surface [19,20,31,32] However, the different types of electrochemical behaviour of Rh and Pt, which are manifested even in the absence of adsorbed CO, were not properly considered in dealing with the differences in the oxidative desorption of CO adsorbates on those metals It should be noted that the H and O adatom electroadsorption potential ranges on Rh in acid are narrower than those on Pt Correspondingly, the potential range for CO and H coadsorption is greater on Rh than on Pt [9], and the overlap of the potential ranges of O adatoms for Rh becomes much larger than for Pt Hence the O electroadsorption on Rh should be strongly inhibited by the presence of CO [20], and the electrodesorption of CO from Rh should depend more strongly on the type of (OH)(CO) lateral interactions than for Pt The shift in the potential of the anodic peak from 0 75 V in acid to 0 95 V in neutral solution (Fig 2C) on polycrystalline Rh sug-

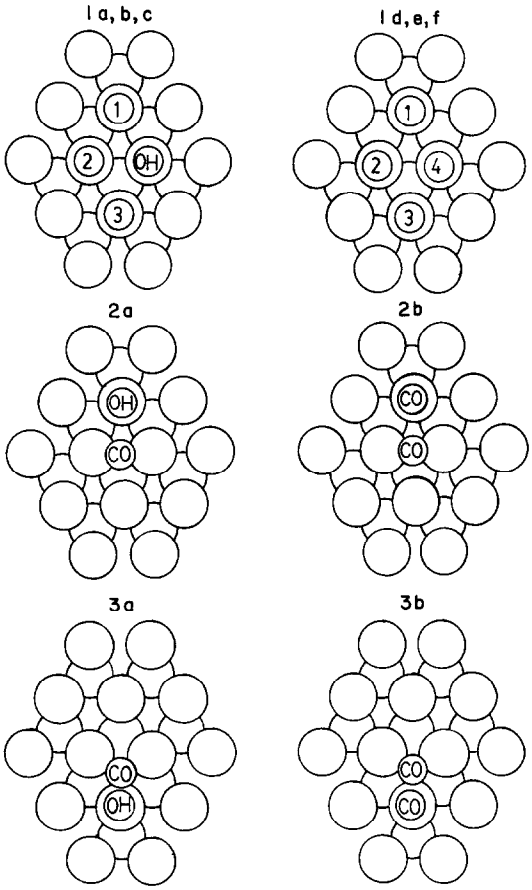

Local structures defined around the central atom of $[Me(111)]_{22}$

	Site 1	Site 2	Site 3	Site 4
(a)	CO	Empty	Empty	–
(b)	CO	CO	Empty	–
(c)	CO	CO	CO	–
(d)	CO	Empty	Empty	CO
(e)	CO	CO	Empty	CO
(f)	CO	CO	CO	CO

Fig 4 Local structures involving the central atoms of the cluster The energies of the various configurations were compared as described in the text in order to define the stability inversion potential (SIP) on Me(111)

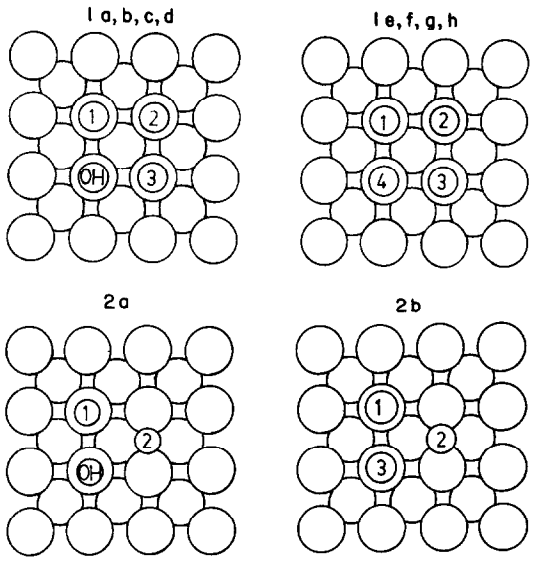

Local structures defined on the central atom of $[Me(100)]_{25}$

	Site 1	Site 2	Site 3
(a)	CO	CO	–
(b)	CO	CO	CO

Fig 5 Local structures involving the central atoms of the cluster The energies of the various configurations were compared as described in the text in order to define the SIP on Me(100)

gests that the (OH)(CO) lateral interactions become largely influenced by the solution composition [29,62]

4. Dependence of the probable CO adsorbate configurations on the electronic characteristics of the metal surface

The possible structures of CO adsorbates on noble metals has been extensively investigated through the C–O stretching frequency, which characterizes the CO/metal surface bonding [28,36,38,46–50] Recently, it was found that the bridge to linear CO–adsorbate interconversion on Pt and Rh cannot be related to similarities in binding energy From the dependence of the spectral frequency on the electric potential measured in situ using IRRAS–EMIRS techniques, it seems more reasonable to assign the CO–adsorbate electrodesorption peak multiplicity on Pt and Rh to potential-induced structural effects [28,63]

The spectral frequency shift was quantitatively interpreted by the application of semi-empirical MO-based ASED calculations [53,64,65] Accordingly, the increase in the CO stretching frequency due to the displacement of CO adsorbates from multiple to single adsorption sites as the potential is positively shifted was explained on the basis of Blyholder's model for CO molecules through a higher stabilization of the 5σ donation to the lower-level metal valence band [53,64–66] Interactions of both σ and π type are known to contribute to the Me–CO bond formation [39–43,63,66] According to ab-initio calculations, σ-type interactions are mainly repulsive (Pauli repulsion) [43,44,63,66] The Me charge in σ-symmetry orbitals hybridizes and polarizes away from CO to reduce the Me–5σ CO overlap and hence to reduce repulsion Otherwise, the π-type interactions are bonding and are the most important in the stabilization of the Me–CO bond Ab-initio [43,44,63,66] density functional [41,42] and semi-empirical [31,32,39] calculations, together with in-situ IR spectroscopy data, demonstrate that linearly coordinated CO adsorbates are present on both Pt and Rh in the potential range where electrodesorption of CO adsorbates takes place Therefore the conclusions derived from the present approach (Fig 6) agree with those reported previously

5. Possible structures involved in the CO electro-oxidation process

Provided that lateral interactions between adsorbed species are involved in the stability of CO adsorbates at any value of θ_{CO}, the electrochemical desorption of CO adsorbates in the aqueous environment should

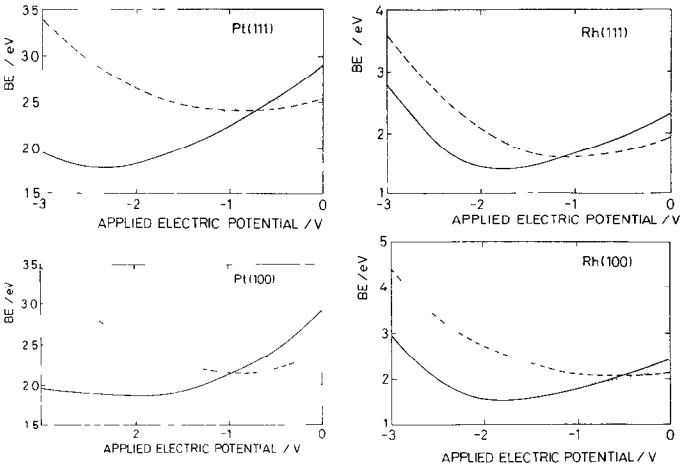

Fig 6 Binding energy (BE) shifts for CO adsorbed on different surfaces sites as a function of the applied potential (positive charging)

occur for a certain potential value at which the stability range of (OH)(CO) coadsorbates is exceeded The threshold potentials related to the electro-oxidation of CO adsorbates have been semi-empirically associated with the stability limits of different adsorbate ensembles represented as $[Me]_N(CO)_n(OH)_m$ ($N = 22$, 25, $n = 1$, 2, 3, $m = 1$, Me = Pt, Rh) At certain applied potentials which depend on the values of m and n, a new $[Me]_N(CO)_{n+m}$ ensemble is formed by displacement of the $(CO_n)(OH)_m$ by $(CO)_{m+n}$ in the adsorption site In terms of the nucleation and growth model, CO adsorbates may belong to either second- or higher-order layers of islands, and in this way the stretching frequency is maintained unshifted through the occupation of sites of the same coordination geometry According to energy calculations, the formation of the $[Me]_N(CO)_{m+n}$ ensemble seems to be more likely than the formation of coadsorbed structures such as CO OH, CO H_2O or COH OH [32]

Spectroscopic data of the Me + CO(gas) system were considered in order to establish the most stable initial adsorbate structure for the different values of θ_{CO}, and to determine how these structures are modified when a positive potential is applied (Figs 7–11) The stability calculations of those structures which were built up on the central four-metal-atom region of each cluster to minimize cluster border effects provide information about the possible local interactions for different values of θ_{CO} (Figs 4 and 5)

At low θ_{CO} values a $(\sqrt{3} \times \sqrt{3})R30°$ LEED CO adsorbate pattern is produced on both Rh(111) and Pt(111) in contact with CO gas through the occupancy of top sites [22,24,25,29,37] (Fig 7), giving rise to the nearest-neighbour interactions depicted in Fig 4 1(a) At intermediate θ_{CO} values either a $c(2 \times 2)$ LEED

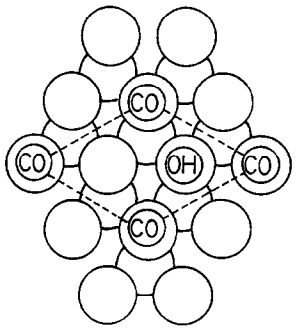

Fig 7 $(\sqrt{3}\times\sqrt{3})R30°$ LEED pattern corresponding to CO adsorbed on Me(111) for $\theta_{CO} = 0\,33$ The possible OH adsorption site is also included The structure of the adsorbed layer remains at positive potential

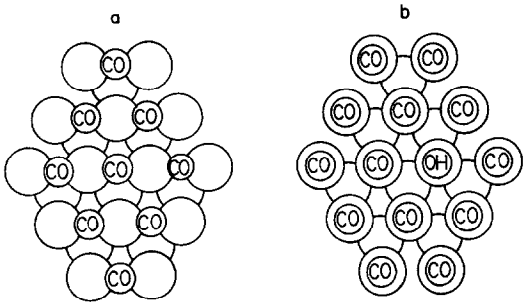

Fig 9 (a) CO adsorbate structures on Me(111) for $\theta_{CO} = 1$, (b) adsorbed structures obtained for a positive potential applied to the initial structure A local vacancy is necessary for OH adsorption

pattern on Rh(111) or a $c(4\times2)$ LEED pattern on Pt(111), implying the simultaneous occupancy of either top and hollow sites or top and bridge sites of the surface respectively, is produced (Fig 8) Different local interactions obtained by changing the adsorption geometry of the CO molecule by a positive applied potential are illustrated in Fig 4 1(a)–4 1(c) Likewise, multibonded CO species would result from the interactions depicted in Figs 4 2 and 4 3 for Pt(111) and Rh(111) respectively However, although the presence of multibonded CO species is rather unlikely on uncharged metals, the stability of these species has also been evaluated

Unfortunately, at present there are no conclusive data related to the structure of CO adsorbates for $\theta_{CO} \Rightarrow 1$ although a positive electrode charging leads to the structure depicted in Fig 9 on both Pt(111) and Rh(111) The interactions involved in the structure illustrated in Fig 4 1(c) favour the desorption of CO

A similar analysis can be extended to Rh(100) and Pt(100) surfaces At low θ_{CO} the CO adsorbate on either Rh(100) or Pt(100) constitutes $c(2\times2)$ LEED patterns through the occupancy of bi-coordinated sites (Fig 10(a)) When a positive potential is applied to these structures, they change to one of those illustrated in Figs 10(b)–10(d) involving configurations such as those depicted in Figs 5 1 and 5 2 As θ_{CO} is increased, the linearly coordinated CO adsorbate on both Rh(100)

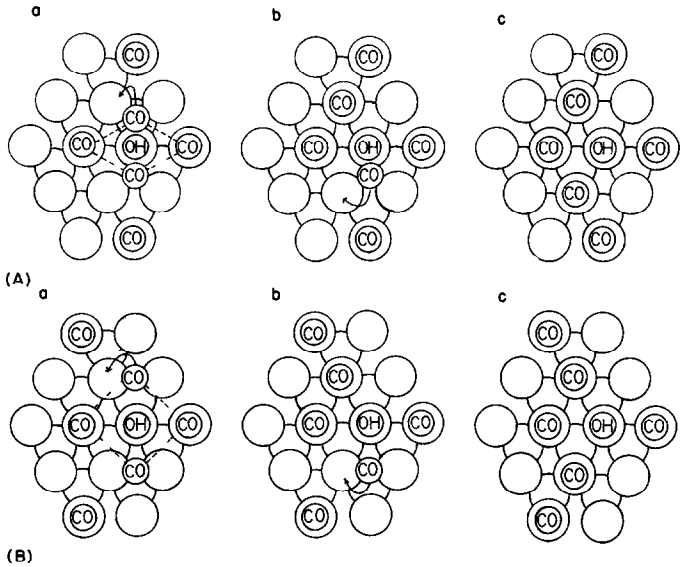

Fig 8 (A) (a) Adsorbed structure derived from the $c(2\times2)$ LEED pattern of CO adsorbed on Rh(111) (uncharged surface) for $\theta_{CO} = 0\,5$, the OH adsorption site is also included, (b), (c) adsorbed structures resulting for a positive potential to the initial $c(2\times2)$ structure (B) (a) Adsorbed structure as derived from the $c(4\times2)$ LEED pattern of CO adsorbed on Pt(111), (b), (c) adsorbed structures obtained by applying a positive potential to the initial $c(4\times2)$ structure

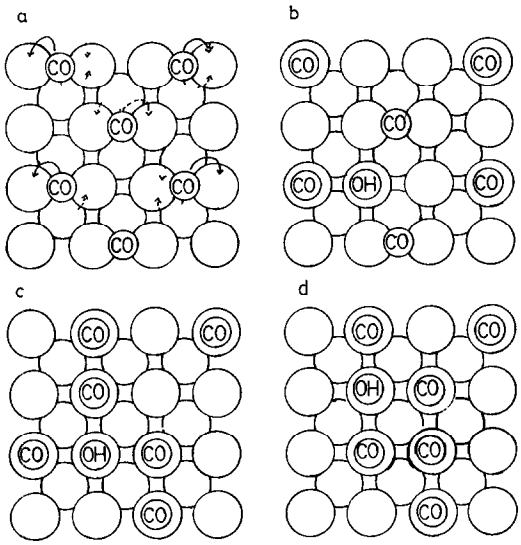

Fig 10 Possible structures of adsorbed CO on Me(100) at $\theta_{CO} = 0\,5$ (a) $c(2\times2)$ LEED pattern derived for the uncharged metal, (b, c, d) possible structure modifications resulting by shifting the potential positively The OH adsorption site is also included

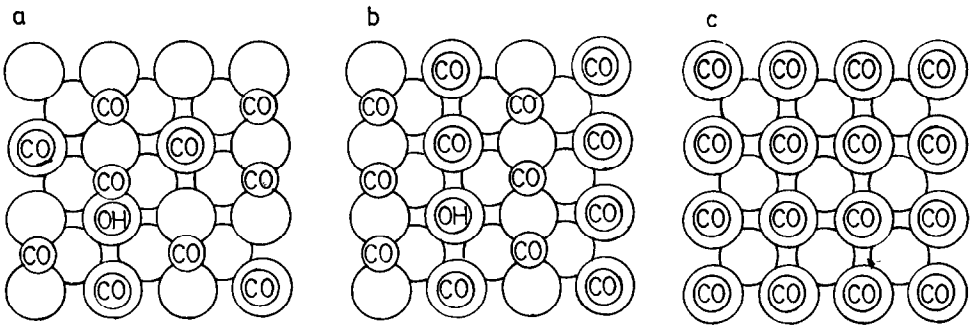

Fig 11 Structures corresponding to relatively high CO surface coverages on Me(100) (a) uncharged surface, Me = Pt, $\theta = 0.65$, $c(2 \times 2)$ LEED pattern, (b) uncharged surface, $\theta = 0.75$, Me = Rh, (2×1) LEED pattern, (c) possible structure resulting from increasing θ_{CO} and shifting the potential positively A local vacancy is required for OH adsorption

and Pt(100) leads to $c(2 \times 1)$ and $c(4 \times 2)$ structures, respectively (Fig 11) Accordingly, under a positive potential and with $\theta_{CO} = 1$, only the interactions resulting for the surface structure depicted in Fig 5 1(c) contribute to the rupture of the adsorbates from both metals

The binding energy levels of the different coadsorbate structures illustrated in Figs 4 1(a)–4 1(c), 4 2(a), 4 3(a), 5 1(a)–5 1(c), 5 2(a) and 5 2(b) change continuously as the applied potential is progressively increased from 0 0 V to 1 0 V, so that these structures become less stable than those shown in Figs 4 1(d)–4 1(f), 4 2(b), 4 3(b), 5 1(d)–5 1(f), 5 2(c) and 5 2(d) The values of BE for adsorbate ensembles for which $n = m = 1$ plotted against the applied potential (Fig 12) indicate that the $[Me]_N(CO)(OH)$ ensemble is the most stable at low potentials, in contrast with the $[Me](CO)_2$ ensemble From these results, it is possible to define the stability inversion potential (SIP) of each ensemble as

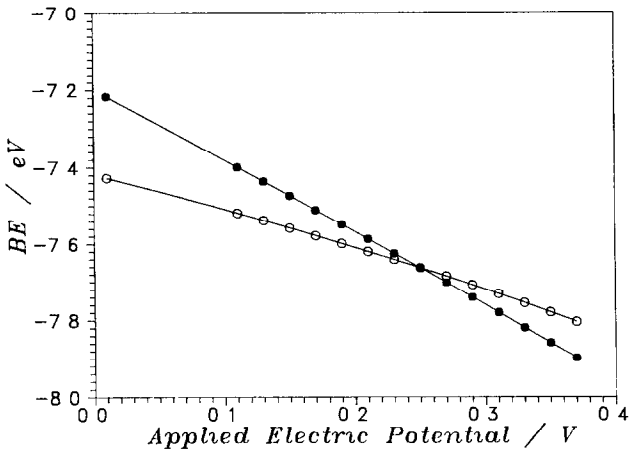

Fig 12 Binding energy of adsorbed (CO) (OH) (○) and of adsorbed $(CO)_2$ (●) ensembles on $[Pt(111)]_{22}$ as a function of the applied electric potential The crossing point of the straight lines determines the SIP

the potential value at which the energy range of the stable structure is exceeded When this occurs the ensemble can change into another form by losing CO_2, according to a process such as

$$[Me]_N(CO)_n(OH) + 2(CO) \Rightarrow [Me]_N(CO)_{n+1} + H^+ + CO_2 + e^- \quad (6)$$

where, as discussed previously, the extra CO molecules in eqn (6) are associated with the adsorbate ensemble or islands in the framework of the nucleation and growth model It should be noted that results from experiments involving $^{12}CO + {}^{13}CO$ mixtures demonstrate that CO electrosorbed on Pt or Rh has the ability to undergo a rapid exchange with solution phase CO [46] These results are consistent with the presence of adsorbate CO structures on the surface

On the assumption that reaction (6) represents the electro-oxidation of the adsorbate, the SIP values related to the different adsorbate configurations can be related to the potentials of the various voltammetric anodic peaks reported for the electro-oxidation of CO adsorbed on Pt(100), Pt(111), Rh(100) and Rh(111) in aqueous acid solutions, provided that the comparison is made at a constant potential sweep v This implies that the various possible reactions involve the same irreversible behaviour as expressed, for instance, through a constant peak potential dependence on v for all reactions [7,8] Accordingly, the theoretical electro-oxidation potential (EOP) corresponding to the voltammetric peaks can be calculated from the SIP values as follows

$$EOP = SIP/g \quad (7)$$

where in this case g, which has been already defined in Section 2, is also a function of the potential sweep rate

The experimental and theoretical EOP values and the values of g employed for the different Pt crystal faces at $v = 10$ V s^{-1} are given in Table 2 A qualitative description of the multiplicity of anodic voltam-

metric peaks for CO adsorbates at low θ_{CO} on both Pt(111) and Pt(100) can be proposed as follows

The voltammetric anodic current peak at 0 81 V on Pt(111) can be assigned to the rupture of adsorbate structures produced at low values of θ_{CO} (Fig 4 1(a)) As the value of θ_{CO} on $[Pt(111)]_{22}$ increases, the voltammetric peak at 0 96 V resulting from the rupture of the $(CO)_2(OH)$ ensemble (Fig 4 1(b)) is observed Subsequently, the peak at 1 10 V can be assigned to the rupture of the $(CO)_3(OH)$ ensemble (Fig 4 1(c)) Finally, bridge-bonded (CO)–(OH) interactions (Figs 4 2(a) and 4 2(b)) give rise to a peak at 1 2 V, which, however, overlaps the oxygen evolution reaction (OER) potential region

The preceding analysis can be extended to $[Pt(100)]_{25}$ for $\theta_{CO} \rightarrow 1$ In this case the peak at 1 08 V can be related to the rupture of the $(CO)_3(OH)$ ensembles (Fig 5 1(d)) Different ensembles can be formed for intermediate values of θ_{CO} under a positive potential (Figs 5 1(b) and 5 1(c)), and their rupture can be related to peaks found at 0 83 V and 0 93 V Furthermore, the adsorbate structures on $[Pt(100)]_{25}$ associated with low values of θ_{CO} (Figs 5 1(a) and 5 2(a)) become unstable only when the applied potential exceeds 0 3 V In this case the residual bridge-bonded CO (Fig 5 2(b)) becomes sufficiently stable up to potentials near the OER threshold potential

Following the same type of analysis for Rh(111), the voltammetric peak at 0 95 V can be assigned to the rupture of the $(CO)_3(OH)$ ensemble (Fig 4 1(c)) for any value of θ_{CO} Nevertheless, for positive charging and low values of θ_{CO} the rupture of the linearly bonded $(CO)_2(OH)$ ensemble (Fig 4 1(b)) would give rise to the anodic current peak at 0 75 V In this case, the CO OH interaction (Fig 4 1(a)) prevailing at low values of θ_{CO} would produce an electro-oxidation peak at 0 47 V which has not been observed

The CO OH adsorbed ensemble on Rh(100) becomes unstable at potentials more positive than those calculated for Rh(111) However, the peak potential related to the rupture of [linearly bonded $(CO)_2$–(OH)] and [linearly bonded (CO)–bridge-bonded (CO)-(OH)] ensembles on Rh(100) (Figs 5 1(b) and 5 2(b)) overlaps that expected from the $(CO)_3(OH)$ ensemble on Rh(111) The same result is obtained for the (CO)(OH) ensemble on Rh(100) (Fig 5 1(d)) and for the $(CO)_2(OH)$ ensemble on Rh(111) Accordingly, the higher stability of the $(CO)_3(OH)$ ensembles on Rh(100) furnishes no extra voltammetric peak Therefore these results explain why CO adsorbates on polycrystalline Rh exhibit an apparent single electro-oxidation current peak

It should be noted that the appearance of the anodic peaks at 0 75 V in acid solution (1 M $HClO_4$, 0 5 M H_2SO_4) and at 0 95 V in neutral solution (0 2 M K_2SO_4), which have been ascribed to CO electro-oxidation from polycrystalline Rh, is consistent with the appearance of two peaks for Rh(100) in 0 1 M $HClO_4$ In addition, a single anodic peak at 0 95 V has also been found for Rh in 1 M $HClO_4$ when $\theta_{CO} \rightarrow 1$ [18,19], with a shoulder at 0 75 V

Since CO cannot displace completely the H adatoms from the Rh surface, either the fourth adsorption site on Rh(111) (Fig 4 1(d)) or both the third and fourth adsorption sites on Rh(100) (Figs 5 1(c) and 5 1(d) are likely to be occupied by H atoms which influence the electro-oxidation characteristics of the CO adsorbate ensembles for low θ_{CO} Accordingly, depending on the CO adsorption time, either voltammetric peaks at 0 95 V and 0 75 V or a single peak at 0 75 V can be observed in acid

From the preceding analysis based upon the shift of the CO adsorbate electro-oxidation peaks to lower potential values, it can be concluded that the occupation of Rh sites by H adatoms would preclude cooperative interactions involving the highest number of nearest-neighbour adsorbed CO molecules on the Rh surface

6. Molecular orbital interpretation

Cooperative interactions resulting from coadsorbed CO and OH species should emerge from molecular orbital interactions between these species and the metal surface [31,32,67] It should be noted that H_2O electrodecomposition yielding adsorbed OH and H^+ ions on both Rh and Pt in acid solution begins at relatively low potentials at which the metal surfaces is already almost covered by linearly bonded CO adsorbates

As can be seen in Fig 13, the stabilization of OH orbitals through bonding interactions occurs in a similar manner on both $[Me]_N(CO)_n$ and $[Me]_N$ substrates However, perturbative interactions involving OH and preadsorbed CO shift the energy of antibonding Me(OH) orbital levels up, this explains why OH becomes more strongly bound to the metal as the number n of CO molecules in the adsorbate ensemble increases Thus, for a given applied potential and metal surface structure (Fig 13), the adsorption energy for OH on $[Me]_N$, $[Me]_N(CO)$, $[Me]_N(CO)_2$ and $[Me]_N(CO)_3$ increases the stability of the coadsorbate ensemble produced by the less effective OH antibonding interaction

However, the Fermi energy level of the metal surface decreases with positive potentials (positive charging) Accordingly, the stability of coadsorbate ensembles decreases on increasing the strength of the antibonding interactions The greater the value of θ_{CO}, the

higher is the electric potential required for the adsorbate electro-oxidative desorption, assuming that it occurs according to reaction (6), when the surface site, which is fully occupied by CO molecules, becomes more stable

The present calculations also show that, as expected, the interactions between constituents within the proper adsorbate ensemble, either $[Me]_N(CO)(OH)$ or $[Me]_N(CO)(CO)$, depend on the distance between the constituents As the interactions between adjacent

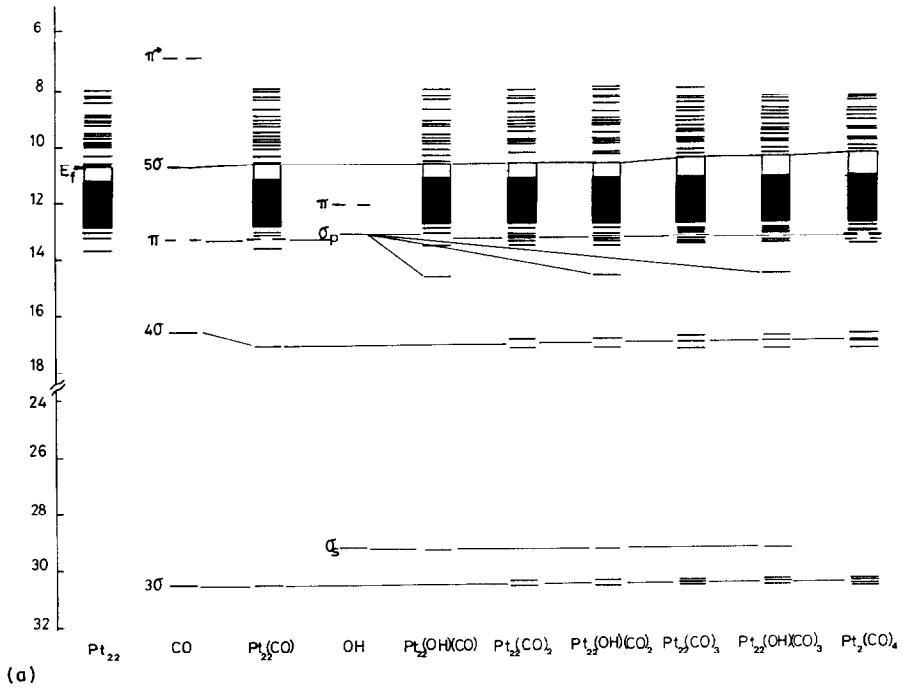

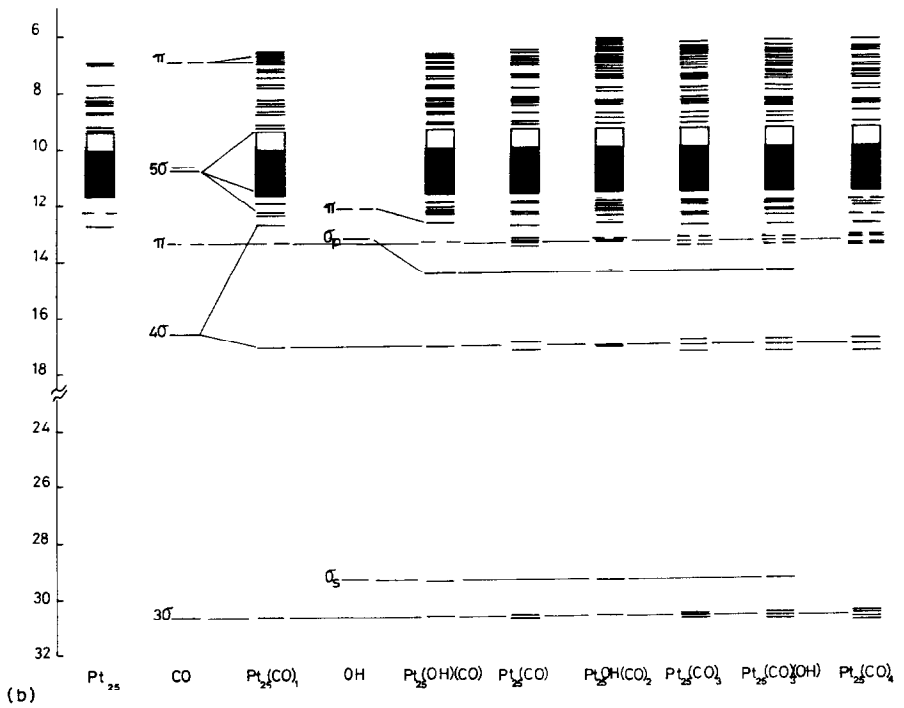

Fig 13 Molecular orbital correlation diagrams for the adsorption and coadsorption of $(CO)_n$ $(0 \leq n \leq 4)$ and (OH) on $[Me]_N$ (a) $[Me]_N = [Pt(111)]_{22}$, (b) $[Me]_N = [Pt(100)]_{25}$, (c) $[Me]_N = [Rh(111)]_{22}$, (d) $[Me]_N = [Rh(100)]_{25}$

CO adsorbates are stronger than those for non-adjacent species, the potential required to electro-oxidize the ensemble shown in Fig 5 1(c) is greater than that required for the electro-oxidation of the ensemble shown in Fig 5 1(b)

However, the dependence of the perturbative inter-

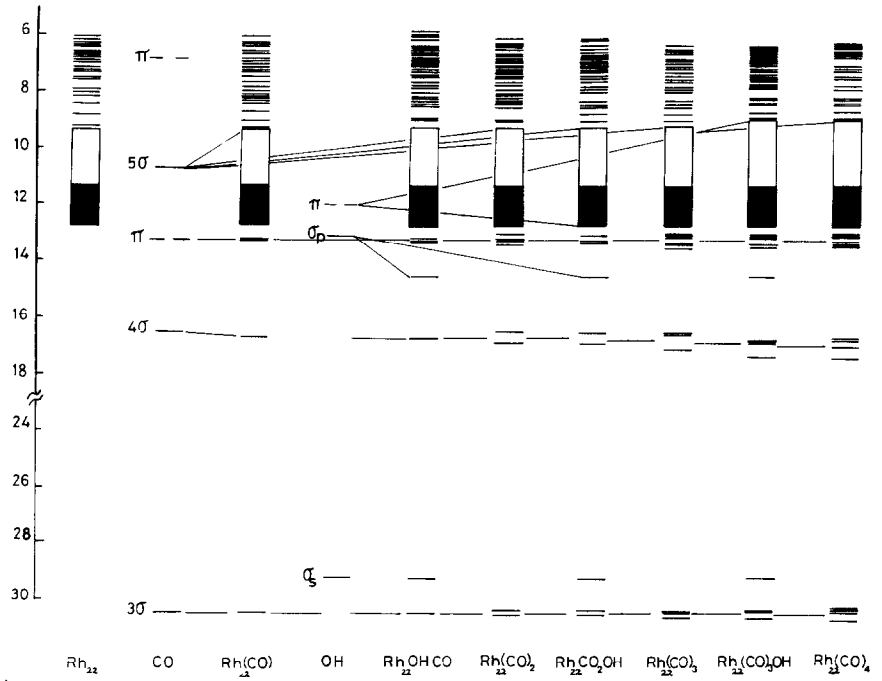

(c)

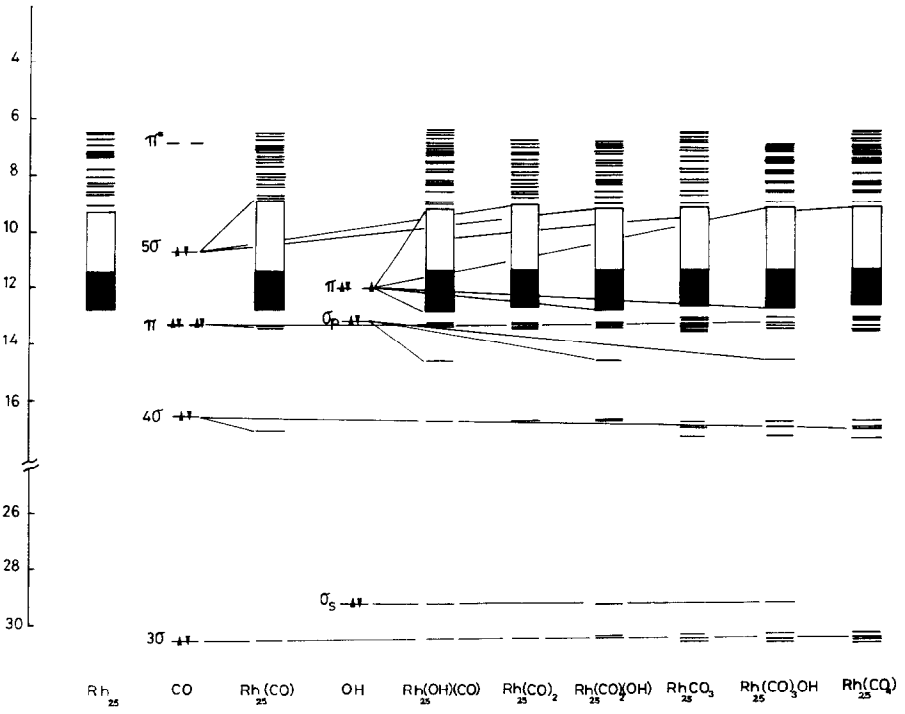

(d)

Fig 13 (continued)

actions on the distance between the ensemble constituents can explain immediately the surprisingly different electro-oxidation potentials of bridge-bonded and linearly bonded CO on Me(100) and Me(111) The perturbative interaction energies resulting for either $[Me]_N$ (bridge-bonded CO)(OH) or $[Me]_N$ (linearly bonded CO)(OH)) on Pt(111) and Rh(111) respectively (Figs 4 2 and 4 3) generate extremely stable ensembles, so that the corresponding electro-oxidation potentials may fall in the potential range where O adatoms rather than OH adsorbed species are formed on both Pt and Rh Accordingly, it seems more reasonable to assign the voltammetric peak at 1 11 V to a surface oxidative adsorbate process involving O adatoms and (CO) adsorbates instead of assigning it to (bridge-bonded CO)(OH) adsorbate

Acknowledgement

The present work was supported by the Consejo Nacional de Investigaciones Científicas y Técnicas of Argentina

References

1 B Beden, A Bewick, K Kunimatsu and C Lamy, J Electroanal Chem , 142 (1982) 345
2 J Léger, B Beden, C Lamy and S Bilmes, J Electroanal Chem , 170 (1984) 305
3 F Kitamura, M Takahashi and M Ito, J Phys Chem , 92 (1988) 3320
4 L Leung, A Wieckowski and M Weaver, J Phys Chem , 92 (1988) 6985
5 S G Sun, J Clavilier and A Bewick, J Electroanal Chem , 240 (1988) 147
6 R Parsons and T VanderNoot, J Electroanal Chem , 257 (1988) 9
7 F Hahn, B Beden and C Lamy, J Electroanal Chem , 258 (1989) 115
8 Z Cataldi, R O Lezna, M C Giordano and A J Arvia, J Electroanal Chem , 261 (1988) 61
9 W Bold and M Breiter, Electrochim Acta, 5 (1961) 145
10 D E Hienhower, H B Urbach and J H Harrison, J Electrochem Soc , 117 (1970) 1500
11 F Wagner and T Moylan, Surf Sci , 206 (1988) 187
12 F Wagner and T Moylan, Surf Sci , 182 (1987) 125
13 F Wagner and T Moylan, Surf Sci , 195 (1988) 403
14 J Clavilier, A Fernández Vega, J M Feliú and A Aldaz, J Electroanal Chem , 263 (1989) 217
15 M Shibata, N Furuya, M Watanabe and S Motoo, J Electroanal Chem , 263 (1989) 97
16 M Shibata and N Furuya, J Electroanal Chem , 269 (1989) 217
17 N Furuya and M Shibata, J Electroanal Chem , 266 (1989) 461
18 S Bilmes, M C Giordano and A J Arvia, J Electroanal Chem , 215 (1987) 183
19 S Bilmes, M C Giordano and A J Arvia, Can J Chem , 66 (1988) 2259
20 S Bilmes, N R de Tacconi and A J Arvia, J Electroanal Chem , 164 (1984) 129
21 K Kunimatsu, R O Lezna and M Enyo, J Electroanal Chem , 258 (1989) 115
22 H Steiniger, S Leeward and H Ibach, Surf Sci , 123 (1982) 264
23 L K Verheij, L Lux, A Anton, B Poetsemand and G Comsa, Surf Sci , 182 (1987) 390
24 A M Lahee, J P Trennies and C Woll, Surf Sci , 177 (1986) 371
25 J Biberian and M Van Hove, Surf Sci , 118 (1982) 443
26 J Biberian and M Van Hove, Surf Sci , 138 (1984) 361
27 Shin-ichi Ishi, Y Ohno and B Viswanathan, Surf Sci , 161 (1985) 349
28 S C Chang, L W H Leving and M J Weaver, J Phys Chem , 93 (1989) 5341
29 S C Chang and M J Weaver, J Electroanal Chem , 285 (1990) 263
30 K Kunimatsu, J Phys Chem , 88 (1984) 2197
31 G L Estiú, S A Maluendes, E A Castro and A J Arvia, J Electroanal Chem , 283 (1990) 303
32 P Paredes Olivera, G L Estiú, E A Castro and A J Arvia, J Mol Struct (THEOCHEM), 210 (1990) 379
33 S A Bilmes and A J Arvia, J Electroanal Chem , 361 (1993) 159
34 J A Caram and C Gutiérrez, J Electroanal Chem , 307 (1991) 99
35 J A Caram and C Gutiérrez, J Electroanal Chem , 305 (1991) 259
36 L H Leung and M J Weaver, J Phys Chem , 93 (1989) 7218
37 L W H Leung, S C Chang and M J Weaver, J Chem Phys , 90 (1989) 7426
38 L H Leung and M J Weaver, J Am Chem Soc , 109 (1987) 5113
39 G L Estiú and M C Zerner, Int J Quantum Chem , 26 (1992) 587
40 G L Estiú and M C Zerner, J Phys Chem , submitted
41 A Goursot, I Papai and D R Salahub, J Am Chem Soc , in press
42 A St Amant, Ph D Thesis, Université de Montreal, 1991
43 P S Bagus, C N Nelin and C W Bauschlicher, Phys Rev B, 28 (1983) 5423
44 C W Bauschlicher, P S Bagus, C N Nelin and B Roos, J Chem Phys , 85 (1986) 354
45 L A Barnes and C W Bauschlicher, J Chem Phys , 91 (1989) 314
46 S C Chang, J D Roth and M J Weaver, Surf Sci , 244 (1991) 113
47 S C Chang and M J Weaver, Surf Sci , 238 (1990) 142
48 S C Chang and M J Weaver, J Chem Phys , 92 (1990) 4582
49 S C Chang and M J Weaver, J Phys Chem , 94 (1990) 5095
50 S C Chang and M J Weaver, Surf Sci , 230 (1990) 222
51 B Love and J Lipkowski, Am Chem Soc Symp Ser , 378 (1988) 489
52 A Anderson, R W Grimes and S Hong, J Phys Chem , 91 (1987) 4245
53 N Ray and A Anderson, Surf Sci , 125 (1983) 803
54 E Clementi and C Roetti, Atomic Data and Nuclear Data Tables, Vol 14, Academic Press, New York, 1974
55 L W Anders, R Hansen and L Bartell, J Chem Phys , 59 (1973) 5277
56 W Lotz, J Opt Soc Am , 60 (1970) 206
57 C Moore, Atomic Energy Levels, NBC Circular 467, National Bureau of Standards, US Government Printing Office, Washington, DC
58 L Pauling, The Nature of the Chemical Bond (3rd edn), Cornell University Press, Ithaca, NY, 1960
59 E Kotz, H Neff and K Muller, J Electroanal Chem , 215 (1986) 33

60 D Kolb, D Rath, R Wille and W Hansen, Ber Bunsenges Phys Chem , 87 (1983) 1108
61 W Boek and D Kolb, Surf Sci , 118 (1982) 613
62 L J Richter, T A Germer and W Ho, Surf Sci 195 (1988) L182
63 G Pachioni and J Koutecky, J Phys Chem , 91 (1987) 2658
64 A Anderson and M Awad, J Am Chem Soc , 107 (1985) 7854
65 P Paredes Olivera, G L Estiú, E A Castro and A J Arvia, J Mol Struct (THEOCHEM), 210 (1990) 351
66 K Herman, P Bagus and C Nelin, Phys Rev B, 35 (1987) 9467
67 P Thiel, E Williams, J Yates and W Weinberg, Surf Sci , 84 (1979) 54